830-H15

NAS1.60:1904

OCT 2 8 1981

NASA Technical Paper 1904

COMPLETED

ORIGINAL

Noise Suppression Characteristics of Peripherally Segmented Duct Liners

Willie R. Watson

SEPTEMBER 1981

NASA

44

NASA Technical Paper 1904

Noise Suppression Characteristics of Peripherally Segmented Duct Liners

Willie R. Watson
Langley Research Center
Hampton, Virginia

NASA
National Aeronautics
and Space Administration

Scientific and Technical
Information Branch

1981

BLANK PAGE

INTRODUCTION

The use of acoustic liners to reduce aircraft engine noise has been the subject of intense investigation by both governmental and industrial groups for over a decade. Figure 1 is an illustration of three types of acoustic liners which have potential noise suppression benefits. Earlier research was concentrated on uniform liners. Recent efforts have centered on axially segmented liners where the liner admittance changes with distance along the duct. There has been little previous work on peripherally segmented liners.

Certain characteristics of axially segmented liners may preclude their application to aircraft engine noise suppression. The optimum design of axially segmented acoustic liners requires an accurate description of the modal distribution of acoustic energy; however, the number of modes generated in a typical aircraft engine is large, and the problem of determining the modal amplitude and relative phasing of these source modes is difficult (if not impossible). Engine nacelles of today's aircraft may not provide sufficient length for the effective use of these liners. Further, axially segmented liners perform best in the lower range of the engine noise spectrum. They do not perform as well in the higher frequency range where greater suppression is needed.

The peripherally segmented liner has a wall admittance which changes in the circumferential direction. These liners may have significant advantages when compared to uniform or axially segmented liners. The duct length is less important because of the fact that segmentation is around the duct circumference instead of along the axis. This is important since high-bypass-ratio engines have inlet ducts with diameters as large as their lengths. Peripherally segmented liners redistribute acoustic energy of a circumferential wave into higher-order circumferential waves and, since these higher order waves are more rapidly attenuated, an improved suppression may result.

Mani (ref. 1) tested a peripherally segmented liner and found that some additional suppression beyond that achieved with a uniform liner could be observed over a broad frequency range. On the basis of this work, he was granted a patent on the concept. However, there has been no extensive experimental testing of this idea. In addition, no theoretical analyses of such liners are available. The separation-of-variables technique cannot be used to obtain the solution for the acoustic field in ducts with peripheral liners. Thus, the solution for the acoustic field in the duct's cross section is more complex than for uniform or axially segmented liners, where separation of variables is possible in the circumferential direction.

Watson (ref. 2) attempted a multimodal, finite-element solution to this problem. However, the number of peripheral strips was severely restricted because of matrix size limitations, and the effects of a realistic sound source could not be evaluated. Abrahamson (ref. 3) attempted a direct numerical solution of the linearized three-dimensional Euler equation with variable-admittance boundary conditions. He concluded that this method could not succeed using present-day computers because of the size and character of the coefficient matrix. Astley et al. (ref. 4) also attacked the problem using a multimodal,

finite-element method, including the effects of an arbitrary mean flow. Astley's approach is subject to the same limitations as the method of reference 2. Thus, there is no available method for computing the acoustic field in ducts with peripherally segmented liners. Such a method is necessary before an evaluation can be made of the effectiveness of circumferential liners as sound attenuators. A method is developed herein which can account for the sound source and a large number of peripheral strips. The primary objectives of this paper are to compute the eigenvalues and eigenfunctions in ducts with peripherally segmented liners and to compare their properties to those of the uniform liner. It is shown how redistribution of the acoustic energy of a single circumferential wave into a multitude of other circumferential waves is a basic physical property of peripherally segmented liners which is not possible for uniform or axially segmented liners. A secondary objective of this paper is to demonstrate the use of uniform-liner eigenfunctions to calculate the eigenvalues and eigenfunctions of peripherally segmented liners. Finally, attenuation characteristics of a peripheral liner are compared to those of an optimal uniform liner for plane-wave sources.

SYMBOLS

a	duct radius
A	amplitude of pressure wave
B	admittance matrix
c	speed of sound
i	unit imaginary number
$I_m( )$	imaginary part of complex expression
J_m	Bessel function of first kind with order m
K	wave number
L	predetermined length over which transmission loss is computed
M	number of m values, $m = 0, 1, \ldots, M-1$
N	number of n values, $n = 0, 1, \ldots, N-1$
N_{mn}	normalization constant for basis function
$P(R,\theta,Z)$	acoustic pressure field
$P_\ell(R,\theta)$	acoustic pressure eigenfunctions
$P_{\ell j}$	coefficients of basis functions in series acoustic pressure eigenfunctions

$Q(R,\theta)$	source pressure
Q_j	coefficients of basis functions in series for source pressure
r,z	dimensional coordinates
R,θ,Z	cylindrical coordinates
Re( )	real part of complex expression
S	number of peripheral strips
[s/N]	integer division of integer s by integer N
T	periodicity of peripherally segmented liner
$\beta(\theta)$	acoustic admittance of duct wall
δ_j	Kronecker delta function
λ	eigenvalue
ρ	ambient density of medium
$\phi_j(\theta)$	basis functions for series expansion of $\beta(\theta)$
$\psi_j(R,\theta)$	basis functions for series expansions of $P_\ell(R,\theta)$ and $Q(R,\theta)$
∇^2	Laplace operator

Subscripts:

j	basis function index
ℓ	eigenfunction index
m	circumferential harmonic number
n	radial (basis) eigenfunction index
s,t	integers

A bar over a symbol denotes a basis function or a constant. A prime denotes the first derivative with respect to distance.

STATEMENT OF PROBLEM

Consider a semi-infinite circular duct with radius a, as shown in figure 2. A lining material with specific acoustic admittance $\beta(\theta)$ is placed along the inner wall, and an initial noise source (such as one generated by an

aircraft engine) is given at $z = 0$. The purpose of the acoustic liner is to attenuate the noise as it propagates along the duct. The mathematical problem is to determine the acoustic field inside the duct. The effectiveness of the lining material may be evaluated from the solution for this field.

Acoustic waves are governed by the Helmholtz equation

$$\nabla^2 P(R,\theta,Z) + K^2 P(R,\theta,Z) = 0 \tag{1}$$

in which a time dependence of the form $e^{-i\omega t}$ has been assumed, $K = \frac{\omega a}{c}$ is the dimensionless wave number, P is the dimensionless acoustic pressure, ω is the angular frequency, t is time, and c denotes the ambient speed of sound. In equation (1), all distances are referred to the duct radius a and the acoustic pressure is referred to the quantity ρc^2 in which ρ is the ambient density of the medium.

The accustic boundary condition along the outer wall ($R = 1$) is expressed in terms of the admittance of the lining material $\beta(\theta)$,

$$\frac{\partial P(R,\theta,Z)}{\partial R} = iK\,\beta(\theta)\,P(R,\theta,Z) \tag{2}$$

At the entrance plane, the boundary condition is assumed known as

$$P(R,\theta,0) = Q(R,\theta) \tag{3}$$

Capital letters are used for dimensionless groups throughout this paper.

Equations (1) to (3) constitute a boundary value problem for the acoustic pressure field $P(R,\theta,Z)$. A solution must be obtained before the effectiveness of the peripheral liner can be evaluated. Analytical solutions to these equations are not available since the acoustic admittance β depends on the azimuthal coordinate θ. Previous attempts at finite element solutions have had limited success because of the size and character of matrices used in the analysis. Thus, an approximate series expansion is used in this paper.

EIGENFUNCTION EXPANSION TECHNIQUE

The solution to equations (1) to (3) is expressed in the form (ref. 2)

$$P(R,\theta,Z) = \sum_{\ell=0}^{2MN-N-1} A_\ell\, P_\ell(R,\theta)\, e^{iK_\ell Z} \tag{4}$$

in which each eigenfunction $P_\ell(R,\theta)$ satisfies a Helmholtz equation

$$\nabla^2 P_\ell(R,\theta) + \lambda_\ell^2 P_\ell(R,\theta) = 0 \tag{5}$$

with the homogeneous boundary conditions

$$\frac{\partial P_\ell(R,\theta)}{\partial R} + iK\,\beta(\theta)\,P_\ell(R,\theta) = 0 \quad \text{at} \quad R = 1 \tag{6}$$

where ∇^2 is the two-dimensional Laplace operator in R and θ. The eigenvalue λ_ℓ is

$$\lambda_\ell^2 = K^2 - K_\ell^2 \tag{7}$$

The eigenfunctions satisfying equations (5) to (7) are also orthogonal. This can be proved using Green's theorem

$$\iint \left(P_\ell\,\nabla^2 P_m - P_m\,\nabla^2 P_\ell\right) dA = \int \left(\frac{P_\ell\,\partial P_m}{\partial R} - \frac{P_m\,\partial P_\ell}{\partial R}\right) dc \tag{8}$$

In view of the fact that both P_m and P_ℓ satisfy equations (5) and (6), equation (8) becomes

$$\left(\lambda_\ell^2 - \lambda_m^2\right) \iint P_\ell P_m\, dA = 0 \tag{9}$$

If $\lambda_\ell \neq \lambda_m$, equation (9) becomes

$$\int P_\ell P_m\, dA = 0 \tag{10}$$

where $m \neq \ell$. Further, the eigenfunctions will be required to form an orthonormal set so that

$$\iint (P_\ell)^2\, dA = 1 \tag{11}$$

Equations (5) to (7) constitute an eigenvalue problem which must be solved before the acoustic field of equation (4) can be determined. In this paper, a numerical solution to this equation is obtained using a second modal expansion for the eigenfunctions $P_\ell(R,\theta)$.

SERIES SOLUTION FOR EIGENFUNCTIONS

To solve the eigenvalue problem for a peripherally segmented liner, a Galerkin method is employed (see ref. 5) which simultaneously considers the field equation (eq. (5)) and the admittance boundary condition (eq. (6)). Solutions of the form

$$P_\ell(R,\theta) = \sum_{s=0}^{2MN-N-1} P_{\ell s}\psi_s(R,\theta) \tag{12}$$

are sought in which

$$\psi_s(R,\theta) = \begin{cases} J_m\left(\bar{\lambda}_{mn}R\right)\Big/\bar{N}_{mn} \cos m\theta & \text{for } s < MN \\ J_m\left(\bar{\lambda}_{mn}R\right)\Big/\bar{N}_{mn} \sin m\theta & \text{for } s \geq MN \end{cases} \tag{13}$$

$$m = \begin{cases} [s/N] & \text{for } s < MN \\ [(s - N - MN)/N] & \text{for } s \geq MN \end{cases} \tag{14}$$

$$n = \begin{cases} s - mN & \text{for } s < MN \\ s - mN - MN - N & \text{for } s \geq MN \end{cases} \tag{15}$$

in which the notation $[s/N]$ denotes integer division of the integer s by the integer N. The normalization constant $\bar{N}_{mn}$ is determined so that the basis functions $\psi_s(R,\theta)$ are orthonormal

$$\bar{N}_{mn}^2 = \iint J_m^2\left(\bar{\lambda}_{mn}R\right)(\cos^2 m\theta)\, dA \tag{16}$$

and the eigenvalues $\bar{\lambda}_{mn}$ are uniform-liner eigenvalues chosen to satisfy the transcendental equation

$$\bar{\lambda}_{mn}\, J_m'\left(\bar{\lambda}_{mn}\right) - iK\bar{\beta}\, J_m\left(\bar{\lambda}_{mn}\right) = 0 \tag{17}$$

The constant admittance $\bar{\beta}$ may be arbitrarily chosen. Two of the possible choices are $\bar{\beta} = 0$, for a hard-wall duct, and $\bar{\beta} = \frac{1}{2\pi}\int_0^{2\pi} \beta(\theta)\, d\theta$, the average value of β for the peripherally segmented liner. The use of these two basis values will be discussed in the following sections.

The unknown coefficients $P_{\ell s}$ are determined by Galerkin's method. Galerkin's condition is

$$\iint \left(\nabla^2 P_\ell + \lambda_\ell^2 P_\ell\right)\psi_t \, dA = 0 \tag{18}$$

where $t = 0, 1, \ldots, 2MN-N-1$. Integrating equation (18) by parts to transfer the Laplace operator to the basis functions ψ_t gives

$$\iint \left(\nabla^2 \psi_t + \lambda_\ell^2 \psi_t\right)P_\ell \, dA = \int \left(\frac{\psi_t \, \partial P_\ell}{\partial R} - \frac{P_\ell \, \partial \psi_t}{\partial R}\right) dc \tag{19}$$

Eliminating $\nabla^2\psi_t$ and $\partial P_\ell/\partial R$ from equation (19) gives

$$\left(\lambda_\ell^2 - \bar{\lambda}_t^2\right)\iint \psi_t P_\ell \, dA = iK \int (\bar{\beta} - \beta) P_\ell \psi_t \, dc \tag{20}$$

and substituting the expansion for P_ℓ into equation (20) gives

$$\lambda_\ell^2 P_{\ell t} = \sum_{s=0}^{2MN-N-1} \left(\delta_{st}\bar{\lambda}_t^2 + B_{ts}\right)P_{\ell s} \tag{21}$$

where

$$B_{ts} = -iK \int (\beta - \bar{\beta})\psi_s \psi_t \, dc \tag{22}$$

Equation (21) determines the vector $P_{\ell s}$ to within an arbitrary constant. This constant is defined through the normalization condition

$$\sum_{s=0}^{2MN-N-1} P_{\ell s}^2 = 1 \tag{23}$$

Equations (21) to (23) represent a system of linear equations which can be solved for the eigenvalue λ_ℓ and series coefficients $P_{\ell s}$ using standard matrix techniques. In this paper, the QR algorithm is employed to obtain the solution to this equation (ref. 6).

CHOICE OF PERIPHERAL LINER AND SOURCE

The source pressure function is usually generated in a hard-wall section. Thus, the source will be specified in terms of hard-wall duct modes. The source pressure function $Q(R,\theta)$ is expanded in the form

$$Q(R,\theta) = \sum_{s=0}^{2MN-N-1} Q_s \psi_s \tag{24}$$

in which the hard-wall basis functions ψ_s are obtained from equation (17) by setting $\bar{\beta} = 0$.

One may also assume that the fabrication of a peripheral liner $\beta(\theta)$ will consist of some sort of periodicity as shown in figure 3. It is assumed that the admittance of the liner repeats after each $\Delta\theta$ on the interval $0 \leq \theta \leq 2\pi$ where $\Delta\theta = \frac{2\pi}{T}$. A liner of this type is referred to as a liner with periodicity T, where T denotes the number of times the liner repeats on the interval $0 \leq \theta \leq 2\pi$. Within each interval, the liner may be subdivided into strips which do not form a repeating pattern.

Because of its periodicity, the admittance function $\beta(\theta)$ is expanded into the fourier series

$$\beta(\theta) = \sum_{s=0}^{\infty} \phi_s \beta_s \tag{25}$$

where

$$\phi_s(\theta) = \begin{cases} \cos mT\theta & \text{for } s \text{ even} \\ \sin mT\theta & \text{for } s \text{ odd} \end{cases} \tag{26}$$

$$m = [(s + 1)/2] \tag{27}$$

EFFECTIVENESS OF LINING MATERIAL

Before proceeding with the solution to equations (5) to (7), it is useful to develop an expression for the attenuation produced by the liner in terms of parameters which have been introduced. The axial acoustic intensity at any axial position in the duct is

$$I(R,\theta,Z) = K^{-1} \mathrm{Re}\left[-iP^* \frac{\partial P}{\partial Z}\right] \tag{28}$$

in which the nondimensional acoustic intensity is referred to ρc^3, Re[ ] denotes the real part of the complex expression enclosed within the brackets, and the superscript asterisk indicates the complex conjugate. The total acoustic power is the integral of the acoustic intensity across the cross section

$$W(Z) = \iint I \, dA \tag{29}$$

and the transmission loss, or decrease in level of the acoustic power from $Z = 0$ to $Z = L$, can be written as

$$TL = 10 \log_{10} \left[W(0)/(W(L)\right] \tag{30}$$

Generally, the specific admittance β is chosen so as to maximize the transmission loss.

In this paper, the eigenmode P_ℓ is expanded in terms of the hard-wall basis functions. These basis functions were chosen not only because the eigenvalues $\bar{\lambda}_{mn}$ are real and appear in standard tables but because the resulting expression for the acoustic power reduces to

$$W(Z) = \sum_{\ell=0}^{2MN-N-1} \sum_{\tilde{\ell}=0}^{2MN-N-1} K^{-1} \mathrm{Re}\left[A_\ell^* A_{\tilde{\ell}} K_\ell I_{\ell\tilde{\ell}} e^{i(K_{\tilde{\ell}} - K_\ell)Z}\right] \tag{31}$$

$$I_{\ell\tilde{\ell}} = \sum_{s=0}^{2MN-N-1} P_{\ell s}^* P_{\tilde{\ell} s} \tag{32}$$

$$A_\ell = \sum_{s=0}^{2MN-N-1} P_{\ell s} Q_s \tag{33}$$

The function $W(Z)$ cannot be simplified to a double summation if $\bar{\beta} \neq 0$.

RESULTS AND DISCUSSION

In this section, eigenvalues and eigenfunctions are presented for uniform and peripherally segmented liners. Emphasis is placed on the solution for the eigenvalue λ_ℓ and the eigenfunction $P_\ell(R,\theta)$ for peripherally segmented liners. The way these solutions change with the number of peripheral strips and the wave number K of the system is of fundamental interest. First, confidence in the analysis is obtained by demonstrating that it agrees with exact results which are possible when the liner admittance is independent of the coordinate θ. Afterward, results are presented for peripherally segmented liners.

Uniform Liners

Analysis.- When the admittance β is independent of the coordinate θ, an exact solution to equations (5) to (7) can be obtained by requiring that $\beta = \bar{\beta}$. Equation (21) becomes

$$\left(\lambda_\ell^2 - \bar{\lambda}_s^2\right) P_{\ell s} = 0$$

where $s = 0, 1, \ldots, 2MN-N-1$. The exact solution to this equation, with the normalization condition, is

$$\lambda_\ell = \bar{\lambda}_s$$

$$P_{\ell s} = \delta_{\ell s}$$

where m and n are related to s by equations (14) and (15). Observe that the solution $P_\ell(R,\theta)$ has the following properties for the uniform liner:

(1) Each eigenfunction is either an even or odd function of θ

(2) The eigenvalues for the even and odd eigenfunctions are identical

(3) Each eigenfunction is composed of only a single function of $m\theta$

These observations are important, since it will be shown in the following section that the eigenfunctions for a peripheral liner will have none of these properties in general. Further, if $\bar{\beta}$ is chosen such that $\bar{\beta} \neq \beta$, then, $B_{ts} \neq 0$ in general and equation (21) cannot be solved exactly (the solution was obtained employing the QR algorithm). However, the solution for the eigenfunctions $P_\ell(R,\theta)$ and eigenvalue λ_ℓ will have the three properties discussed earlier. These three properties are preserved because the matrix equation which governs equation (22) when $\beta \neq \bar{\beta}$ is block diagonal, with each diagonal block giving the solution for either an even or odd eigenfunction. This eigenfunction is composed of only a single function of $m\theta$.

Now consider the eigenfunction expansion of the acoustic field as given by equation (4). The modal coefficient A_ℓ is

$$A_\ell = \iint Q(R,\theta)\, P_\ell(R,\theta)\, dA = \sum_{s=0}^{2MN-N-1} P_{\ell s} Q_s$$

Now for uniform liners, A_ℓ is zero for any standing wave (cos $m\theta$ or sin $m\theta$) not present at the source. Thus, for uniform liners, the acoustic energy in an even standing wave of the source remains in that even standing wave in the lined section. This is also true for odd standing waves. It is not possible, therefore, to redistribute the energy of a single standing wave of the source into a

multitude of standing waves in the lined section with a uniform liner. In addition the uniform liner restricts the energy in even standing waves of the source to even waves in the lined section. Similarly, the energy in odd standing waves of the source is restricted to odd standing waves in the lined section. In the next section, it is shown that peripherally segmented liners do allow the redistribution of acoustic energy out of even standing waves of the source into even and odd standing waves in the lined section. It is also shown that peripherally segmented liners allow the redistribution of acoustic energy out of a given standing wave of the source into a multitude of standing waves in the lined section. These properties of peripherally segmented liners may make them better attenuators of sound than uniform liners.

Eigenvalue computation.- Attention is now focused on the eigenvalues computed from the present analysis and how they approximate the exact eigenvalues satisfying equation (17). In order to compare the two solutions, equation (17) has been solved using a Newton-Raphson iterative procedure (ref. 7) with $\beta = \bar{\beta}$. Results for uniform liners will be restricted to optimum liners for plane-wave sources where the optimum values of β have been taken directly from the results of Lester and Posey (ref. 8). All uniform liner results are for $m = 0, 1, 2$ and $N = 10$.

Table I allows comparison of eigenvalues computed from equation (21) to those computed from solving the exact transcendental equation for $m = 0$ with $K = 2$. Note that the present analysis computes the eigenvalues with the larger magnitudes more accurately than those with the smaller magnitudes. This is not surprising since lower-order eigenvalues can be expected to have more simple mode shapes than higher-order ones. Thus, it can be expected that more terms are needed in a Bessel function series to represent functions which are closer to plane waves. Overall, the agreement between the exact eigenvalues and those of the present analysis ranges from one to four significant figures.

Eigenvalues are presented in tables II and III for $m = 1$ and $m = 2$, respectively. Values of K and β are identical to those of table I. The trends of these tables are consistent with those of table I.

Results are presented in table IV for a nondimensional wave number of $K = 5$ for $m = 0$. Eigenvalues computed from equation (21) compare favorably with those computed from the exact transcendental equation. Computations for $m = 1$ and $m = 2$ are given in tables V and VI, respectively. The value of the admittance β is identical to that of table IV. These results show that better comparison is obtained at this higher value of K. The eigenvalues computed in tables IV, V, and VI agree to within two to three significant figures with those of the exact transcendental equation.

Computations have also been obtained for $K = 10$. These results are shown in tables VII, VIII, and IX for $m = 0$, 1, and 2, respectively. Results in these tables are consistent with those of the previous tables. The highest order eigenvalues are computed more accurately than the lower order ones. Again, agreement between the eigenvalues computed from the exact equation and those of the present analysis is within two to three significant figures.

Overall, the agreement between the eigenvalues tends to improve with increasing wave number K and mode order ℓ.

Eigenfunctions.- Attention is now focused on the characteristic functions $P_\ell(R,\theta)$ computed from the analysis presented in this work. As in any acceptable approximate formulation, the series solution computed here must converge in some sense to the exact solution of the problem. Because basis functions used here are for $\bar{\beta} = 0$, the expansion given by equation (12) cannot possibly satisfy the boundary conditions at the outer wall. It is useful to study the effects of this choice of basis functions on the approximate solution. Further, since the circumferential dependence of each eigenfunction will match for a uniform liner, only the radial dependence of the eigenfunctions will be studied.

The real and imaginary parts of the $\ell = 0$ mode for $K = 2$ are plotted in figures 4 and 5, respectively. Agreement between this analysis and the exact analysis is poor for this lowest order mode. Results for the $\ell = 4$ and $\ell = 9$ modes are shown in figures 6 to 9 for $K = 2$. The results for these higher-order modes are virtually indistinguishable from the exact results, even at the boundary. In general, the higher the mode number, the more accurately this analysis computes the eigenfunction.

The real and imaginary parts of the $\ell = 0$ mode for $K = 10$ are plotted in figures 10 and 11, respectively. At this higher value of K, this lowest-order mode is in good agreement with the exact value. Results for the $\ell = 4$ and $\ell = 9$ modes are given in figures 12 to 15 for this higher value of K. Results computed from this analysis are identical to the exact values for these higher-order modes.

Characteristic functions have also been computed for $K = 3, 4, 5, 6, 7,$ and 8 for various values of ℓ. Results for these will not be presented for the sake of brevity. However, trends show that the accuracy of the modes computed from this analysis increases with increasing K, with the lowest-order mode being less accurate than higher-order ones.

Attention is now focused on the radial derivative of the characteristic function $P_\ell(R,\theta)$. How the radial derivative computed from this analysis compares with the exact value is of special interest because of the fact that the hard-wall duct modes are used as basis functions. Recall that the radial derivatives computed from this analysis cannot compare with the exact value at the boundary unless $\beta = 0$, or $P_\ell(1,\theta) = 0$.

The real and imaginary parts of $\partial P_\ell/\partial R$ for the $\ell = 0$ mode are plotted in figures 16 and 17, respectively, for $K = 2$. Overall, values computed from this analysis do not compare to the exact values for this lowest-order mode. Further, results computed from this analysis are less accurate as the outer boundary ($R = 1$) is approached.

Results for the real and imaginary parts of $\partial P_\ell/\partial R$ for the $\ell = 4$ and $\ell = 9$ modes are plotted in figures 18 to 21 for $K = 2$. Results for these higher-order modes are virtually indistinguishable from the exact values, with the exception of the outer boundary ($R = 1$).

Shown in figures 22 and 23 are results for $\partial P_\ell/\partial R$ for $\ell = 0$ with $K = 10$. Observe that the analysis used here computes the radial derivative of P_ℓ more accurately at this higher value of K than at $K = 2$. Overall, this lower-order mode has not been accurately computed by this analysis at this higher K, and the accuracy decreases as the boundary $R = 1$ is approached.

Results for the real and imaginary parts of $\partial P_\ell/\partial R$ for the $\ell = 4$ and $\ell = 9$ mode are plotted in figures 24 to 27 for $K = 10$. Results for these higher-order modes are in good agreement with the exact values except near the outer boundary.

Transmission losses.- In this section, the transmission losses predicted from equations (30) to (33) for optimum uniform liners are compared to results predicted from the analysis of reference 8. The source pressure distribution was assumed to be a plane wave so that $Q(R,\theta) = 1$. The duct geometry was chosen so that the length to diameter ratio was unity ($L = 2$).

Transmission losses are presented in figure 28. The transmission loss spectrum is given for a frequency range $2 \leq K \leq 20$. The losses predicted from the analysis of this work are identical to those of the method of reference 8 for $K > 4$. However, for $K < 4$, the transmission losses predicted from this analysis are less than those predicted in reference 8. As the frequency decreases, the difference between the two curves in figure 28 increases.

The discrepancies between the transmission losses at low frequencies ($K < 4$) predicted from this analysis and from that of reference 8 are not surprising. Thus, for $K < 4$, only the $\ell = 0$ mode is cut on in the duct (ref. 8). However, the analysis of this work cannot accurately resolve the $\ell = 0$ mode at low frequencies.

Peripherally Segmented Liners

Analysis.- Attention is now focused on peripherally segmented liners. To understand why the eigenfunction $P_\ell(R,\theta)$ for a peripheral liner has properties fundamentally different from those of a uniform liner, the basic structure of equation (21) is studied when β is a function of the coordinate θ. In this instance, the matrix of coefficients β_{ts} is not block diagonal as for the uniform liner. As a consequence, the energy in either an even or odd mode of the source is redistributed into other even and odd modes in the lined section. This also results in the generation of a multitude of standing waves for each eigenfunction $P_\ell(R,\theta)$. As a consequence, the energy in a single standing wave of the source is redistributed into a multitude of standing waves in the lined section of the duct. The results of this section will show that this does indeed occur.

Now the number of unknowns in equation (21) will be large. For example, the order of this matrix equation will be 190 if $M = 10$ and $N = 10$. However, if the function $\beta(\theta)$ is restricted to an even function, $B_{ts} = B_{st} = 0$ for $s > MN$ and $t \leq MN$. As a result, the eigenfunction $P_\ell(R,\theta)$ will be composed of either even or odd modes. Further, if the source produces only even modes,

only the even functions need be included in equation (12) and the order of the system is reduced by (MN - N). Thus, results in this section are restricted to admittance functions which are even and, in addition, the source is assumed to be composed of only even modes. Results of the previous section also show that 10 radial modes (N = 10) appear to be sufficient in the series expansion of equation (12) for uniform liners. The number of radial modes has been terminated at N = 10 for peripherally segmented liner results. Note also that up to this point there is no rule for choosing the number of standing waves in the expansion given by equation (12). Finally, since $\beta(\theta)$ is assumed an even function, $\beta(\theta) = \beta(2\pi - \theta)$ and the form of $\beta(\theta)$ need only be specified on the interval $(0,\pi)$. Results for peripheral liners are restricted to a liner having a periodicity of one (T = 1) in which the admittance segments alternate between β_1 and β_2 with a given number of strips S on the interval $(0,\pi)$, as shown in figure 29.

Eigenvalues.- Table X contains eigenvalues for a two-strip liner (S = 2) for various values of M. The liner admittance has been taken as $\beta_1 = 1.54 - 1.29i$ and $\beta_2 = 0.0 + 0.0i$ with the dimensionless frequency K chosen as 2. These results show that the eigenvalues are significantly different for the lower values of M, but do converge as M increases. In fact, there is very little change in the first 10 eigenvalues when M is increased from 6 to 10. Table XI contains eigenvalues for K = 5, with all other parameters identical to those of table X. The effects of M at this higher value of K are consistent with those at the lower value of K. Eigenvalues have also been computed for K = 4, 6, 8, and 10, and the effects of increasing M were always consistent with those of tables X and XI.

The effects of varying the number of strips on the eigenvalues of peripheral liners for K = 2 and K = 5 are shown in tables XII and XIII, respectively. Values of β_1 and β_2 employed in the two tables are identical to those of table X, and 10 standing waves have been employed (M = 10). It is clear from these two tables that the number of strips affects the eigenvalues and subsequently the eigenmodes $P_\ell(R,\theta)$ even though the amount of the duct which is acoustically treated for each configuration is still 50 percent. Thus, the attenuation properties of peripherally segmented liners will depend on the number of peripheral strips, even if the amount of lined section is kept fixed.

Eigenfunctions.- The analysis presented in this work can also be used to investigate the eigenfunctions of peripherally segmented liners. Valuable insight about the eigenfunctions can be obtained by studying the coefficients $P_{\ell s}$ which go into the series expansion for the eigenfunction $P_\ell(R,\theta)$ in equation (12). In table XIV the coefficients $P_{\ell s}$ computed for the $\ell = 0$ mode of table XII are shown. Only values of ℓ which correspond to $n = 0$ are shown (i.e., each value of s corresponds to a different order standing wave). The first column of coefficients in this table is for the uniform liner for which $\beta_1 = \beta_2 = 1.54 - 1.29i$ and for the same value of K as the peripheral liner. Results of table XIV confirm that the peripheral liner generates a multitude of standing waves regardless of the number of segments. This is borne out by the fact that $P_{\ell s} \neq 0$ for any s for the peripheral liners. Contrast this to the uniform liner coefficients in which $P_{\ell s} = 0$ for $s \neq 0$.

Results similar to those of table XIV have been computed for other values of ℓ in addition to $\ell = 0$ and for other values of K, β_1, and β_2. For each value of ℓ, the peripheral liner eigenfunction $P_\ell(R,\theta)$ consisted of a multitude of standing waves, while the uniform liner contains only one standing wave. Thus, the multimodal expansion of the acoustic field for peripherally segmented liners (eq. (4)), will contain a multitude of standing waves for any given source.

Transmission losses.- Baseline trends for the transmission loss of a peripherally segmented liner are given by the attenuation of the least attenuated mode (this would correspond to setting $A_\ell = 0$ in eq. (33) for $\ell \neq 0$). The attenuation of the least attenuated mode is $-8.69\ \mathrm{Im}(K_0 L)$ dB in which Im( ) denotes the imaginary part of the complex expression within the parentheses and dB denotes decibels of sound.

The attenuation of the least-attenuated mode $\ell = 0$ is assumed to provide a rough estimate of the transmission loss for the peripheral liner. This attenuation would equal the transmission loss if the duct was infinitely long and the mode $\ell = 0$ carried all the acoustic energy. Figure 30 allows comparison of these attenuations for uniform and peripherally segmented liners for $L = 1$. The uniform liner is chosen so that the attenuation is optimum at $K = 3$ (this implies an admittance of $\beta = 0.81 - 0.73i$); whereas, the peripherally segmented liner is chosen so that $\beta_1 = 0.81 - 0.78i$ and $\beta_2 = 0$. Results of figure 30 show that peripheral liners with a small number of strips ($S = 2$ and $S = 4$) have poor attenuations compared to the uniform liner. The $S = 6$ and $S = 10$ liners attenuate more for frequencies >3.5 than the uniform liner. This is rather surprising, since only 50 percent of the duct wall is treated with peripheral strips; whereas, the uniform liner covers the entire wall. Peripheral liners with a large number of strips have broader attenuation characteristics than uniform liners, and the peak attenuation occurs at a higher frequency. These characteristics may be a significant advantage for actual engine sources which produce noise over a wide frequency range.

Turning now to the effects of the sound source, figure 31 is a comparison of transmission losses for an optimum uniform liner to those of an arbitrarily chosen peripherally segmented liner. Results in this figure are for a plane-wave source ($Q = 1$) with $L = 2$. The uniform liner is optimum at $K = 5$ so that $\beta = 0.34 - 0.59i$ for this liner (ref. 8). The admittances of the peripheral liner are chosen such that $\beta_1 = 0.40 - 0.59i$ and $\beta_2 = 0.5 - 0.2i$. The transmission loss was computed from equations (30) to (33). Both peripherally segmented liners give transmission losses comparable to that of the uniform liner for $K \leq 6$ and for $K \geq 17$. For values of K between these values, the peripheral liner gives greater transmission losses than the uniform liner for this plane-wave source. Further, the $S = 4$ peripheral liner gives a 50-percent increase in the attenuation over the uniform liner for $K = 8$.

CONCLUSIONS

An analysis method has been developed for computing the acoustic field and transmission losses in ducts with peripherally segmented liners, arbitrary

sources, and any number of peripheral strips. Based upon this work, the following conclusions are made:

(1) Peripherally segmented liners redistribute the energy in standing waves composed of only a single circumferential mode at the source into other waves which contain a multitude of circumferential modes in the lined section.

(2) The accuracy of the eigenvalues and eigenfunctions computed from this analysis increases with both the frequency and the mode order.

(3) Transmission losses computed from this analysis were determined to be accurate for wave numbers greater than four, which is the approximate cut-on value of the first order radial mode in a hard-wall duct.

(4) Results based on the attenuation of the least-attenuated mode show that peripherally segmented liners can attenuate more sound over a broader frequency range than a uniform liner, although 50 percent of the peripheral liner was hard wall.

(5) Finally, results show that, for a plane-wave source, a nonoptimal peripherally segmented liner may attenuate as much sound as an optimized uniform liner at the optimal point, while giving more noise suppression at other frequencies. These results lend credence to the concept of a peripherally segmented liner and encourage further analysis utilizing optimized peripherally segmented liners and more realistic sources.

Langley Research Center
National Aeronautics and Space Administration
Hampton, VA 23665
August 5, 1981

REFERENCES

1. Mani, Ramani: Acoustic Duct With Peripherally Segmented Acoustic Treatment. U.S. Pat. 3, 937,590, Feb. 10, 1976.

2. Watson, Willie R.: A Finite Element Simulation of Sound Attenuation in a Finite Duct With a Peripherally Variable Liner. NASA TM-74080, 1977.

3. Abrahamson, A. L.: A Feasibility Study of a 3-D Finite Element Solution Scheme for Aeroengine Duct Acoustics. NASA CR-159359, 1980.

4. Astley, R. J.; Walkington, N. J.; and Eversman, W.: Transmission in Flow Ducts With Peripherally Varying Linings. AIAA-80-1015, June 1980.

5. Finlayson, Bruce A.: The Method of Weighted Residuals and Variational Principles With Application in Fluid Mechanics, Heat and Mass Transfer. Academic Press, Inc., c.1972.

6. Strang, Gilbert: Linear Algebra and Its Applications. Academic Press, Inc., c.1976.

7. Zorumski, William E.: Acoustic Theory of Axisymmetric Multisectional Ducts. NASA TR R-419, 1974.

8. Lester, Harold C.; and Posey, Joe W.: Optimal One-Section and Two-Section Circular Sound-Absorbing Duct Liners for Plane-Wave and Monopole Sources Without Flow. NASA TN D-8348, 1976.

TABLE I.- EIGENVALUES AT OPTIMUM ADMITTANCE FOR PLANE-WAVE SOURCE

($K = 2$, $\beta = 1.54 - 1.29i$)

Radial mode number, ℓ	Exact solution to transcendental equation: $\lambda_\ell J_0'(\lambda_\ell) - 2i\beta J_0(\lambda_\ell) = 0$	Numerical solution computed from solving equation (21)
0	2.885 - 0.489i	2.950 - 0.461i
1	3.062 - 3.083i	2.740 - 3.120i
2	6.592 - .422i	6.600 - .373i
3	9.902 - .299i	9.903 - .265i
4	13.122 - .230i	13.121 - .204i
5	16.310 - .186i	16.309 - .165i
6	19.482 - .157i	19.481 - .138i
7	22.645 - .135i	22.644 - .117i
8	25.803 - .119i	25.802 - .101i
9	28.957 - .106i	28.956 - .087i

TABLE II.- EIGENVALUES AT OPTIMUM ADMITTANCE FOR PLANE-WAVE SOURCE

($K = 2$, $\beta = 1.54 - 1.29i$)

Radial mode number, ℓ	Exact solution to transcendental equation: $\lambda_\ell J_1'(\lambda_\ell) - 2i\beta J_1(\lambda_\ell) = 0$	Numerical solution computed from solving equation (21)
10	3.146 - 3.041i	2.860 - 3.070i
11	4.683 - .534i	4.720 - .476i
12	8.199 - .359i	8.202 - .320i
13	11.473 - .263i	11.472 - .235i
14	14.684 - .207i	14.683 - .185i
15	17.869 - .171i	17.868 - .152i
16	21.040 - .146i	21.039 - .129i
17	24.204 - .127i	24.203 - .111i
18	27.362 - .112i	27.361 - .096i
19	30.517 - .101i	30.516 - .083i

TABLE III.- EIGENVALUES AT OPTIMUM ADMITTANCE FOR PLANE-WAVE SOURCE

($K = 2$, $\beta = 1.54 - 1.29i$)

Radial mode number, ℓ	Exact solution to transcendental equation: $\lambda_\ell J_2'(\lambda_\ell) - 2i\beta J_2(\lambda_\ell) = 0$	Numerical solution computed from solving equation (21)
20	3.537 - 2.876i	3.277 - 2.860i
21	6.203 - .485i	6.216 - .433i
22	9.680 - .318i	9.680 - .286i
23	12.962 - .238i	12.961 - .214i
24	16.183 - .191i	16.182 - .171i
25	19.377 - .159i	19.376 - .142i
26	22.555 - .137i	22.554 - .121i
27	25.725 - .120i	25.723 - .105i
28	28.888 - .107i	28.886 - .092i
29	32.046 - .096i	32.045 - .092i

TABLE IV.- EIGENVALUES AT OPTIMUM ADMITTANCE FOR PLANE-WAVE SOURCE

($K = 5$, $\beta = 0.34 - 0.59i$)

Radial mode number, ℓ	Exact solution to transcendental equation: $\lambda_\ell J_0'(\lambda_\ell) - 5i\beta J_0(\lambda_\ell) = 0$	Numerical solution computed from solving equation (21)
0	3.058 - 0.277i	3.096 - 0.260i
1	1.668 - 3.485i	1.476 - 3.370i
2	6.589 - .217i	6.609 - .194i
3	9.881 - .159i	9.894 - .141i
4	13.101 - .124i	13.111 - .109i
5	16.291 - .101i	16.299 - .089i
6	19.465 - .086i	19.422 - .074i
7	22.630 - .074i	22.637 - .064i
8	25.790 - .065i	25.796 - .055i
9	28.945 - .058i	28.953 - .047i

TABLE V.- EIGENVALUES AT OPTIMUM ADMITTANCE FOR PLANE-WAVE SOURCE

(K = 5, $\beta = 0.34 - 0.59i$)

Radial mode number, ℓ	Exact solution to transcendental equation: $\lambda_\ell J_1'(\lambda_\ell) - 5i\beta J_1(\lambda_\ell) = 0$	Numerical solution computed from solving equation (21)
10	4.744 - 0.268i	4.772 - 0.244i
11	1.790 - 3.354i	1.615 - 3.226i
12	8.182 - .188i	8.197 - .168i
13	11.450 - .141i	11.461 - .126i
14	14.663 - .112i	14.672 - .100i
15	17.851 - .093i	17.858 - .082i
16	21.024 - .080i	21.031 - .070i
17	24.190 - .070i	24.196 - .060i
18	27.350 - .062i	27.356 - .052i
19	30.505 - .055i	30.512 - .045i

TABLE VI.- EIGENVALUES AT OPTIMUM ADMITTANCE FOR PLANE-WAVE SOURCE

(K = 5, $\beta = 0.34 - 0.59i$)

Radial mode number, ℓ	Exact solution to transcendental equation: $\lambda_\ell J_2'(\lambda_\ell) - 5i\beta J_2(\lambda_\ell) = 0$	Numerical solution computed from solving equation (21)
20	2.157 - 2.930i	2.003 - 2.770i
21	6.212 - .264i	6.234 - .223i
22	9.658 - .169i	9.671 - .152i
23	12.940 - .128i	12.949 - .115i
24	16.164 - .104i	16.171 - .092i
25	19.360 - .087i	19.366 - .077i
26	22.540 - .075i	22.546 - .066i
27	25.711 - .066i	25.717 - .057i
28	28.875 - .059i	28.881 - .050i
29	32.035 - .053i	32.042 - .043i

TABLE VII.- EIGENVALUES AT OPTIMUM ADMITTANCE FOR PLANE-WAVE SOURCE

($K = 10, \quad \beta = 0.21 - 0.45i$)

Radial mode number, ℓ	Exact solution to transcendental equation: $J_0'(\lambda_\ell) - 10i\beta J_0(\lambda_\ell) = 0$	Numerical solution computed from solving equation (21)
0	2.865 - 0.194i	2.912 - 0.185i
1	6.395 - .219i	6.439 - .191i
2	9.736 - .179i	9.769 - .152i
3	2.086 - 5.024i	1.742 - 4.713i
4	12.988 - .145i	13.013 - .121i
5	16.198 - .121i	16.220 - .100i
6	19.387 - .103i	19.406 - .084i
7	22.573 - .090i	22.580 - .072i
8	25.730 - .079i	25.748 - .062i
9	28.892 - .071i	28.911 - .052i

TABLE VIII.- EIGENVALUES AT OPTIMUM ADMITTANCE FOR PLANE-WAVE SOURCE

($K = 10, \quad \beta = 0.21 - 0.45i$)

Radial mode number, ℓ	Exact solution to transcendental equation: $J_1'(\lambda_\ell) - 10i\beta J_1(\lambda_\ell) = 0$	Numerical solution computed from solving equation (21)
10	4.521 - 0.232i	4.571 - 0.211i
11	8.011 - .202i	8.048 - .175i
12	2.142 - 4.927i	1.816 - 4.618i
13	11.321 - .162i	11.349 - .138i
14	14.561 - .133i	14.583 - .112i
15	17.766 - .112i	17.785 - .091i
16	20.952 - .096i	20.969 - .079i
17	24.126 - .084i	24.142 - .068i
18	27.293 - .075i	27.309 - .059i
19	30.455 - .068i	30.473 - .050i

TABLE IX.- EIGENVALUES AT OPTIMUM ADMITTANCE FOR PLANE-WAVE SOURCE

($K = 10$, $\beta = 0.21 - 0.45i$)

Radial mode number, ℓ	Exact solution to transcendental equation: $J_2'(\lambda_\ell) - 10i\beta J_2(\lambda_\ell) = 0$	Numerical solution computed from solving equation (21)
20	5.994 - 0.239i	6.041 - 0.213i
21	9.504 - .188i	9.536 - .162i
22	2.323 - 4.628i	2.019 - 4.291i
23	12.822 - .150i	12.846 - .128i
24	16.069 - .124i	16.089 - .104i
25	19.280 - .105i	19.297 - .087i
26	22.472 - .091i	22.487 - .075i
27	25.651 - .080i	25.666 - .065i
28	28.822 - .072i	28.836 - .057i
29	31.987 - .065i	32.003 - .048i

TABLE X.- EIGENVALUES FOR TWO-STRIP PERIPHERALLY SEGMENTED LINER

($T = 1$, $S = 2$, $K = 2$, $\beta_1 = 1.54 - 1.29i$, $\beta_2 = 0.0 + 0.0i$)

ℓ	M				
	1	3	5	6	10
0	1.363 - 1.918i	1.346 - 0.339i	1.276 - 0.254i	1.285 - 0.230i	1.289 - 0.228i
1	3.450 - .388i	2.484 - 1.283i	2.826 - 3.044i	2.823 - 3.046i	2.825 - 3.048i
2	6.824 - .209i	2.830 - 3.044i	3.323 - .374i	3.300 - .326i	3.295 - .325i
3	10.044 - .144i	3.416 - .266i	3.710 - .471i	3.581 - 2.393i	3.599 - 2.414i
4	13.225 - .109i	5.041 - .213i	3.638 - 2.369i	3.817 - .311i	3.830 - .323i
5	16.391 - .088i	6.483 - .231i	4.616 - .684i	5.044 - .212i	5.045 - .212i
6	19.549 - .074i	6.813 - .188i	5.045 - .209i	5.024 - 1.552i	5.179 - 1.559i
7	22.703 - .063i	8.370 - .153i	6.469 - .230i	5.765 - .409i	5.851 - .628i
8	25.853 - .055i	9.831 - .150i	6.810 - .190i	6.483 - .195i	6.514 - .190i
9	29.002 - .048i	10.039 - .134i	7.810 - .180i	6.813 - .183i	6.817 - .179i

TABLE XI.- EIGENVALUES FOR TWO-STRIP PERIPHERALLY SEGMENTED LINER

(T = 1, S = 2, K = 5, β_1 = 1.54 - 1.29i, β_2 = 0.0 + 0.0i)

ℓ	M				
	1	3	5	6	10
0	2.815 - 0.388i	1.352 - 0.124i	1.319 - 0.142i	1.258 - 0.126i	1.281 - 0.113i
1	3.346 - 3.786i	3.159 - .147i	3.111 - .149i	3.083 - .148i	3.088 - .143i
2	6.478 - .442i	4.786 - .158i	3.971 - .204i	3.765 - .238i	3.869 - .193i
3	9.828 - .314i	3.681 - 3.579i	4.796 - .151i	4.793 - .157i	4.796 - .153i
4	13.067 - .244i	6.108 - .442i	4.561 - 3.024i	5.404 - .355i	5.651 - .345i
5	16.266 - .198i	6.516 - .215i	6.101 - .290i	6.211 - .247i	6.330 - .186i
6	19.446 - .166i	5.950 - 6.938i	6.516 - .211i	6.533 - .212i	6.566 - .193i
7	22.614 - .141i	8.130 - .198i	5.959 - 6.944i	5.960 - 6.939i	5.959 - 6.945i
8	25.776 - .121i	9.611 - .315i	6.362 - 6.624i	6.477 - 5.563i	6.377 - 6.634i
9	28.934 - .103i	9.816 - .219i	7.544 - .205i	6.392 - 6.567i	7.557 - .182i

TABLE XII.- EFFECT INCREASING NUMBER OF STRIPS HAS ON EIGENVALUES OF PERIPHERALLY SEGMENTED LINER (T = 1, K = 2, β_1 = 1.54 - 1.29i, β_2 = 0.0 + 0.0i)

ℓ	S		
	2	4	10
0	1.289 - 0.228i	2.046 - 0.768i	1.568 - 1.770i
1	2.825 - 3.048i	2.504 - .678i	2.224 - 1.715i
2	3.295 - .325i	2.982 - 2.808i	2.978 - 1.539i
3	3.599 - 2.414i	3.393 - 2.013i	3.476 - .479i
4	3.830 - .323i	3.912 - .265i	3.917 - 1.313i
5	5.045 - .212i	5.063 - .275i	4.888 - 1.208i
6	5.179 - 1.559i	5.098 - 1.202i	5.138 - .355i
7	5.851 - .628i	5.926 - 1.033i	5.813 - .704i
8	6.514 - .190i	6.529 - .173i	6.524 - .283i
9	6.817 - .179i	6.836 - .167i	6.844 - .252i

TABLE XIII.- EFFECT INCREASING NUMBER OF STRIPS HAS ON EIGENVALUES OF PERIPHERALLY SEGMENTED LINER (T = 1, K = 5, β_1 = 1.54 - 1.29i, β_2 = 0.0 + 0.0i)

ℓ	S		
	2	4	10
0	1.281 - 0.113i	1.869 - 0.332i	2.603 - 0.453i
2	3.088 - .143i	2.885 - .351i	3.895 - .768i
3	3.869 - .193i	4.154 - .394i	4.882 - .663i
4	4.796 - .153i	4.697 - .248i	5.656 - 1.024i
5	5.651 - .345i	6.077 - .862i	4.732 - 3.420i
6	6.330 - .186i	6.296 - .226i	5.982 - .953i
7	6.566 - .193i	6.664 - .302i	5.625 - 3.190i
8	5.959 - 6.945i	6.814 - 1.011i	6.396 - .809i
9	6.377 - 6.634i	6.092 - 6.825i	6.864 - .604i
10	7.557 - .182i	6.381 - 6.390i	6.576 - 4.165i

TABLE XIV.- REDISTRIBUTION OF ENERGY INTO MULTIPLE STANDING WAVES BY PERIPHERALLY SEGMENTED LINER (T = 1, K = 2, β_1 = 1.54 - 1.29i, β_2 = 0.0 + 0.0i)

Series coefficients, $P_{\ell s}$	Uniform liner values	Peripheral liner with 2 strips (S = 2)	Peripheral liner with 4 strips (S = 4)	Peripheral liner with 10 strips (S = 10)
P_{000}	0.213 + 0.188i	-0.347 - 0.188i	-0.063 + 0.266i	0.525 + 0.000i
P_{010}	.000 + .000i	.834 + .000i	-.340 - .336i	-.301 + .337i
P_{020}	.000 + .000i	-.200 + .208i	.539 + .000i	-.238 - .094i
P_{030}	.000 + .000i	.187 - .028i	-.275 - .347i	-.015 + .124i
P_{040}	.000 + .000i	.001 - .084i	.077 - .075i	-.115 - .024i
P_{050}	.000 + .000i	.067 - .084i	.155 + .197i	.004 + .087i
P_{060}	.000 + .000i	.014 - .027i	-.006 + .009i	-.086 + .017i
P_{070}	.000 + .000i	-.027 + .031i	.005 - .036i	.015 + .094i
P_{080}	.000 + .000i	-.010 - .010i	-.018 + .045i	-.092 - .034i
P_{090}	.000 + .000i	.014 - .021i	-.018 + .008i	.039 + .272i

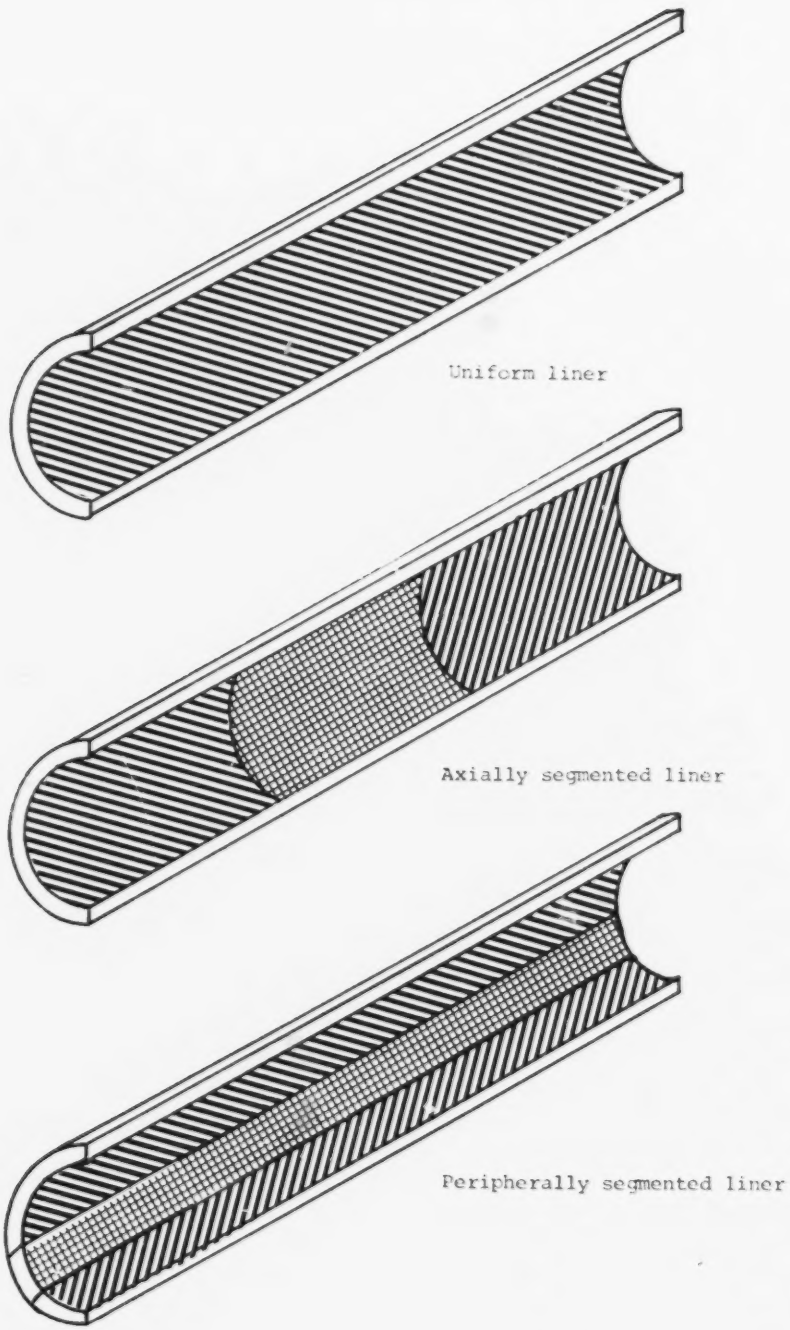

Figure 1.- Duct liner concepts.

Figure 2.- Semi-infinite circular duct.

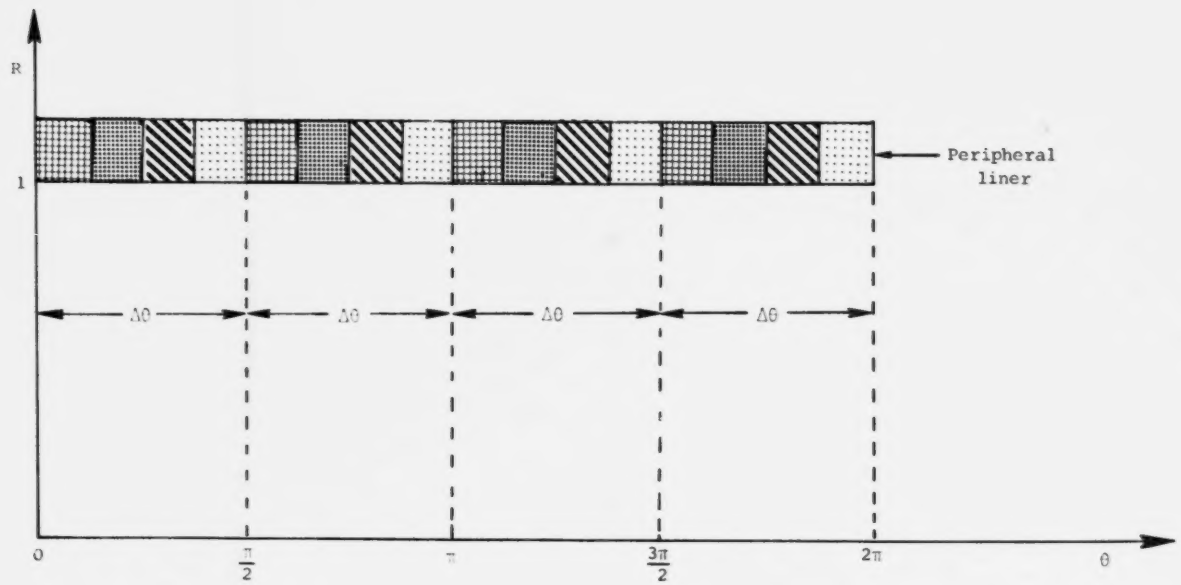

Figure 3.- Peripheral liner with periodicity of T = 4.

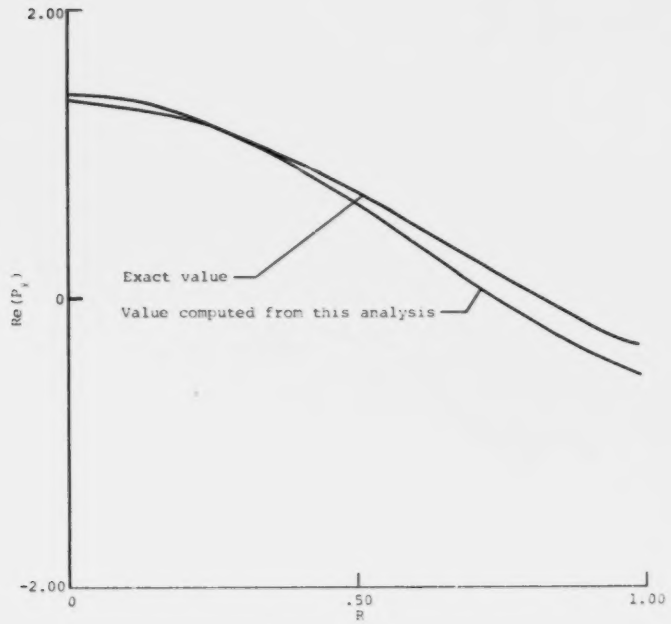

Figure 4.- Real part of $\ell = 0$ radial mode for $K = 2$, $\beta = 1.54 - 1.29i$, and $\lambda_\ell = 2.885 - 0.4889i$.

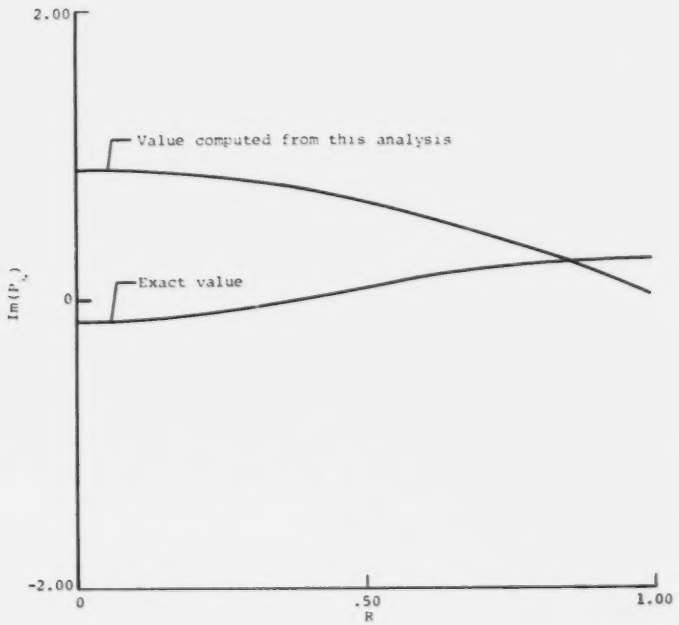

Figure 5.- Imaginary part of $\ell = 0$ radial mode for $K = 2$, $\beta = 1.54 - 1.29i$, and $\lambda_\ell = 2.885 - 0.4889i$.

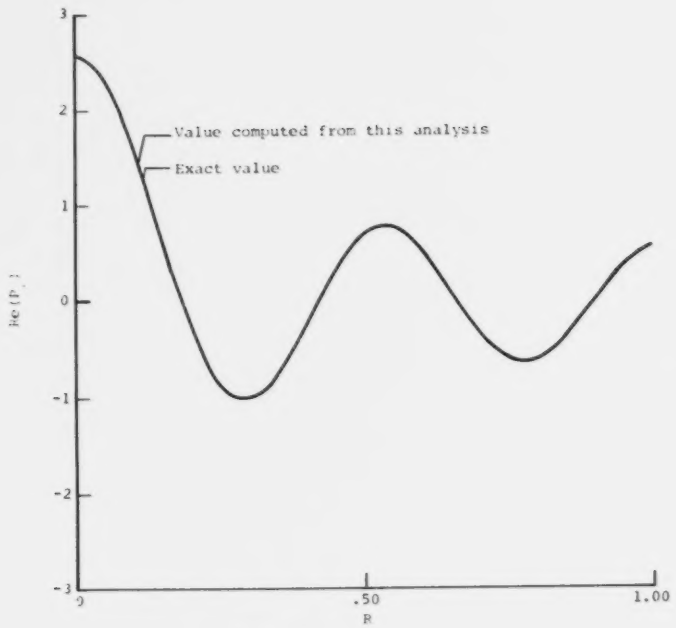

Figure 6.- Real part of $\ell = 4$ radial mode for $K = 2$, $\beta = 1.54 - 1.29i$, and $\lambda_\ell = 13.122 - 0.23i$.

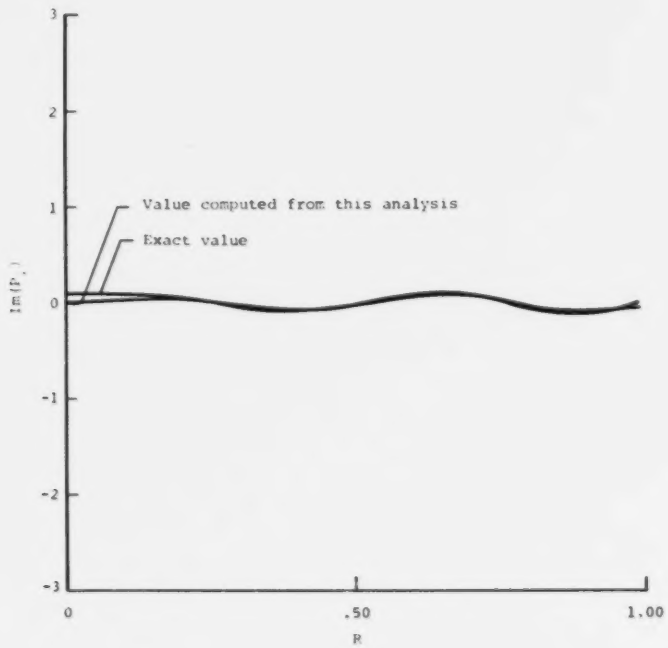

Figure 7.- Imaginary part of $\ell = 4$ radial mode for $K = 2$, $\beta = 1.54 - 1.29i$, and $\lambda_\ell = 13.122 - 0.23i$.

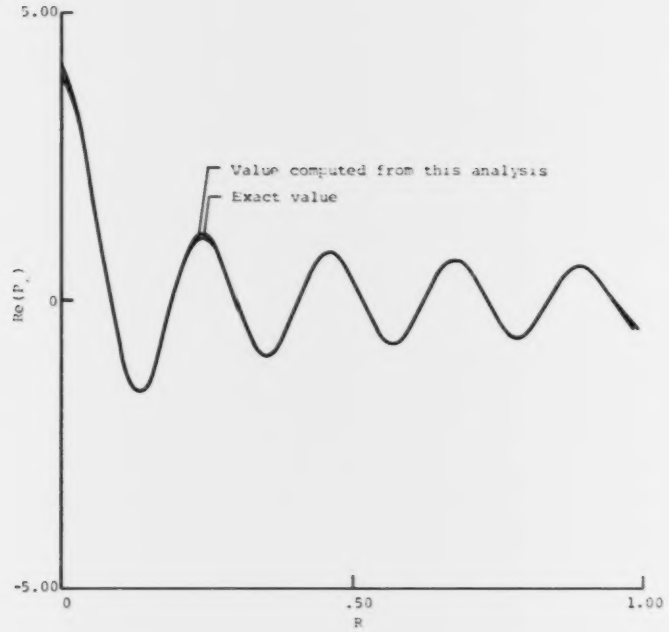

Figure 8.- Real part of $\ell = 9$ radial mode for $K = 2$, $\beta = 1.54 - 1.29i$, and $\lambda_\ell = 28.957 - 0.106i$.

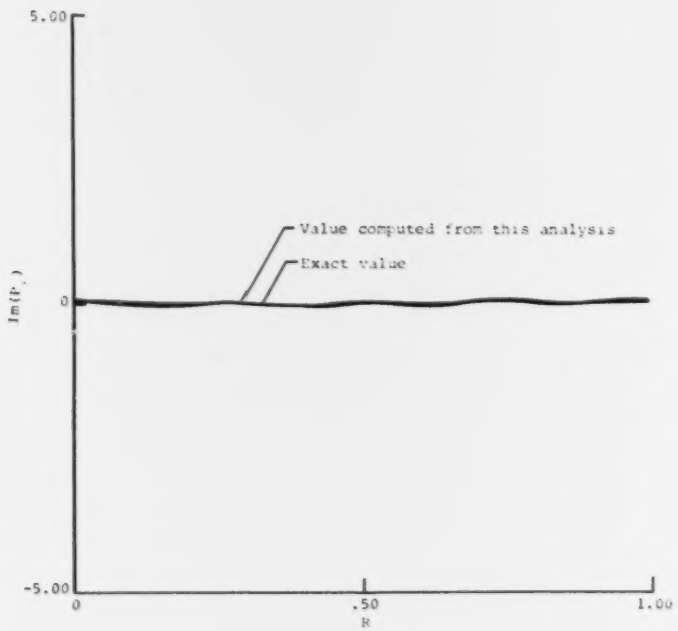

Figure 9.- Imaginary part of $\ell = 9$ radial mode for $K = 2$, $\beta = 1.54 - 1.29i$, and $\lambda_\ell = 28.957 - 0.106i$.

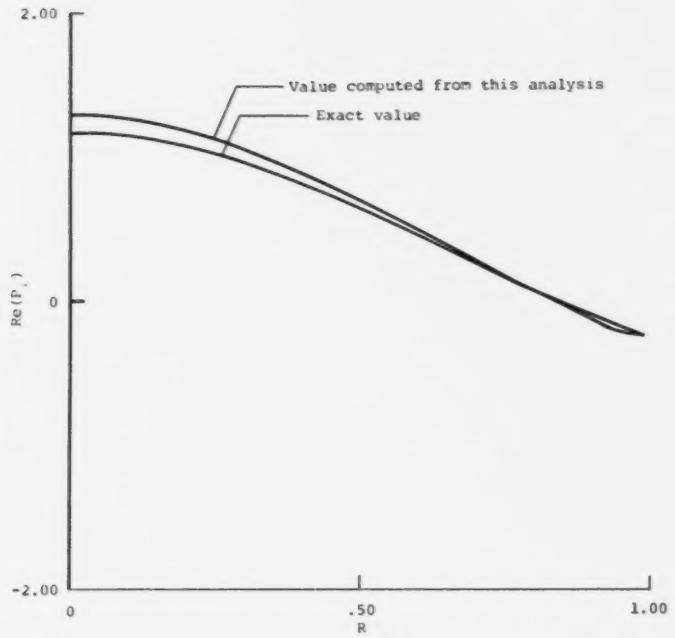

Figure 10.- Real part of $\ell = 0$ radial mode for $K = 10$, $\beta = 0.21 - 0.45i$, and $\lambda_\ell = 2.865 - 1.94i$.

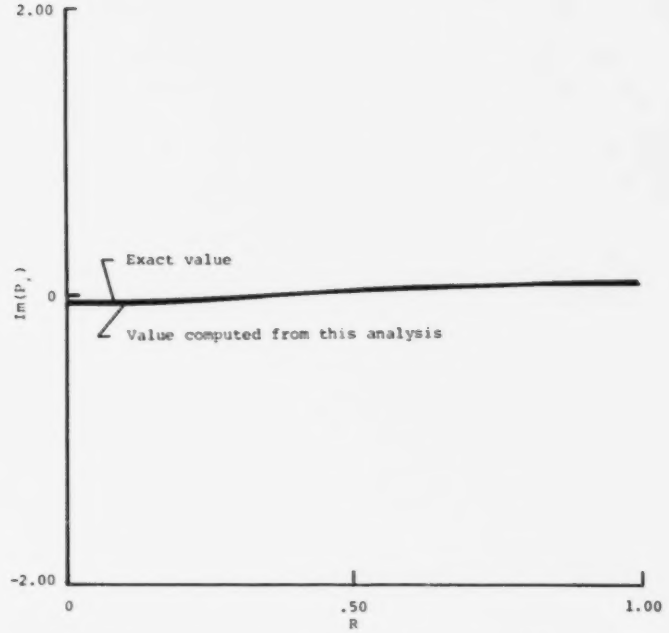

Figure 11.- Imaginary part of $\ell = 0$ radial mode for $K = 10$, $\beta = 0.21 - 0.45i$, and $\lambda_\ell = 2.865 - 1.94i$.

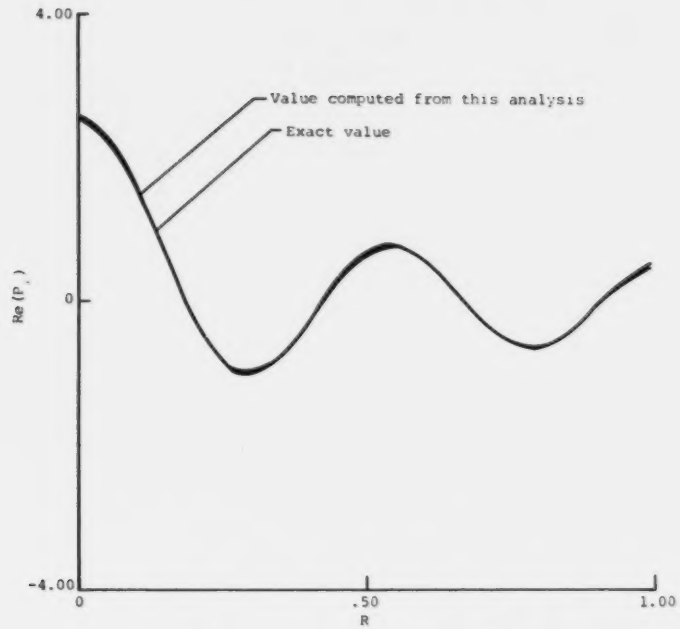

Figure 12.- Real part of $\ell = 4$ radial mode for $K = 10$, $\beta = 0.21 - 0.45i$, and $\lambda_\ell = 12.988 - 0.145i$.

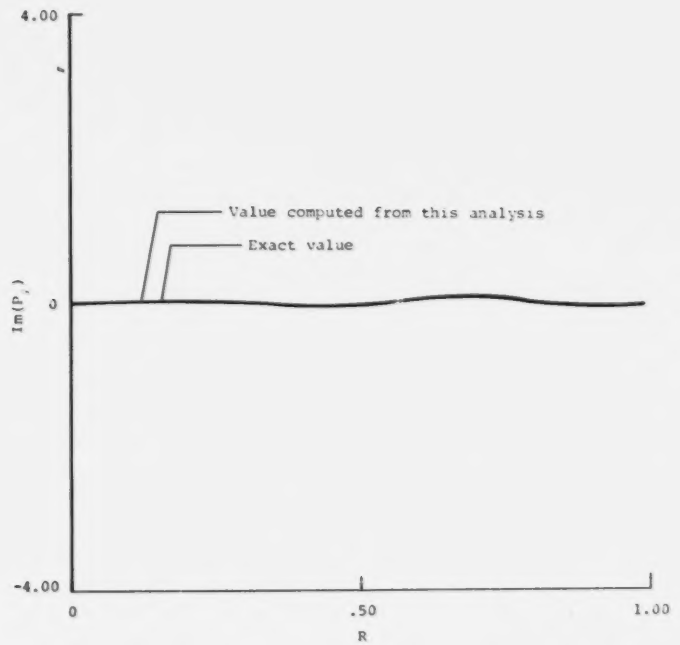

Figure 13.- Imaginary part of $\ell = 4$ radial mode for $K = 10$, $\beta = 0.21 - 0.45i$, and $\lambda_\ell = 12.988 - 0.145i$.

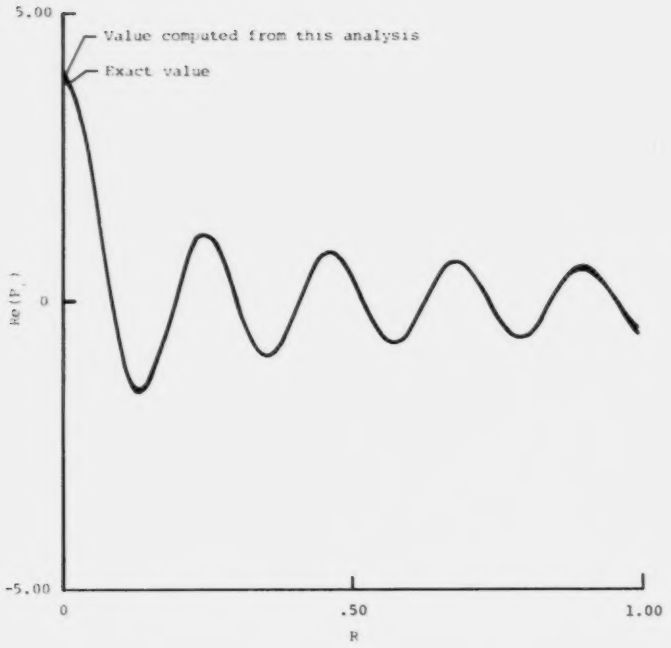

Figure 14.- Real part of $\ell = 9$ radial mode for $K = 10$, $\beta = 0.21 - 0.45i$, and $\lambda_\ell = 28.892 - 0.071i$.

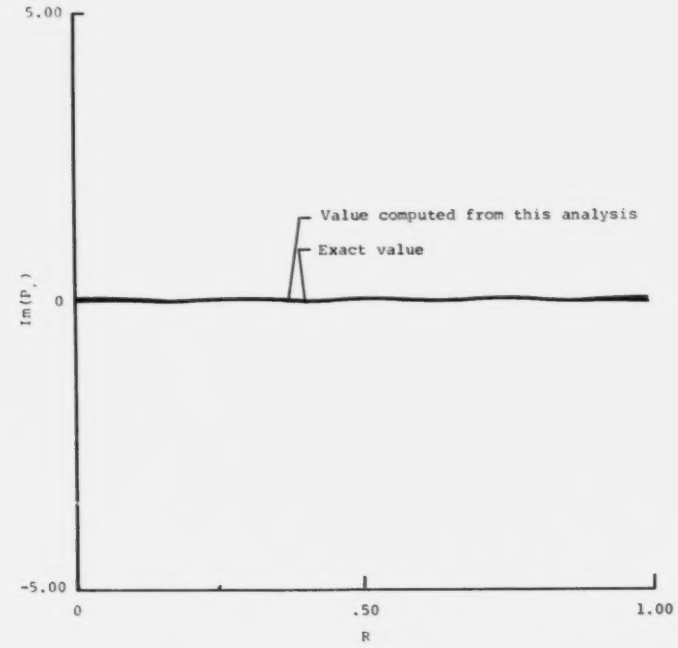

Figure 15.- Imaginary part of $\ell = 9$ radial mode for $K = 10$, $\beta = 0.21 - 0.45i$, and $\lambda_\ell = 28.892 - 0.071i$.

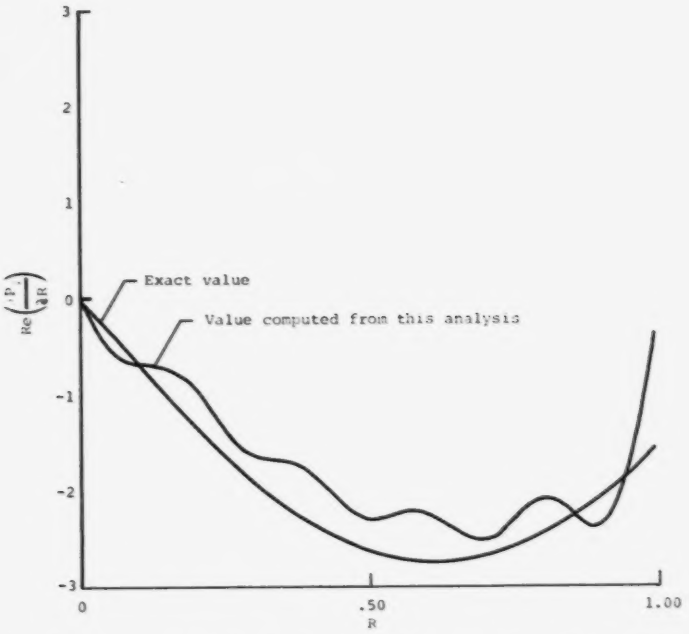

Figure 16.- Real part of radial derivative of the $\ell = 0$ radial mode for $K = 2$, $\beta = 1.54 - 1.29i$, and $\lambda_\ell = 2.885 - 0.4889i$.

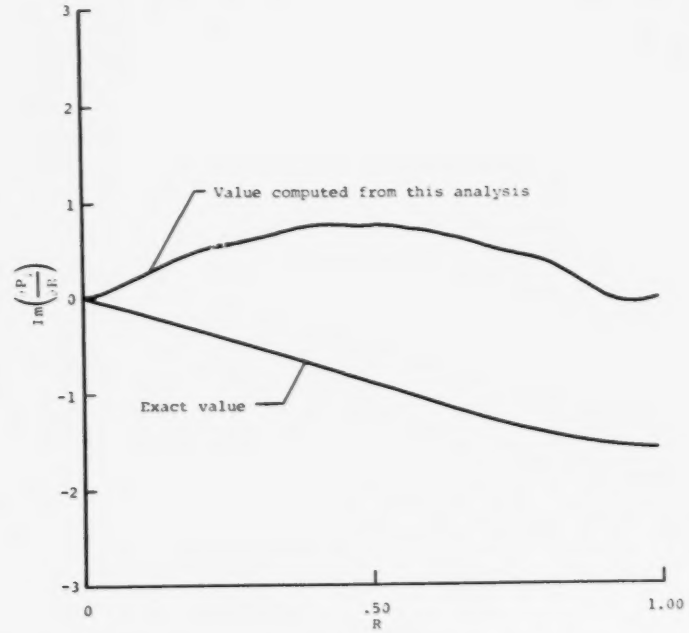

Figure 17.- Imaginary part of radial derivative of the $\ell = 0$ radial mode for $K = 2$, $\beta = 1.54 - 1.29i$, and $\lambda_\ell = 2.885 - 0.4889i$.

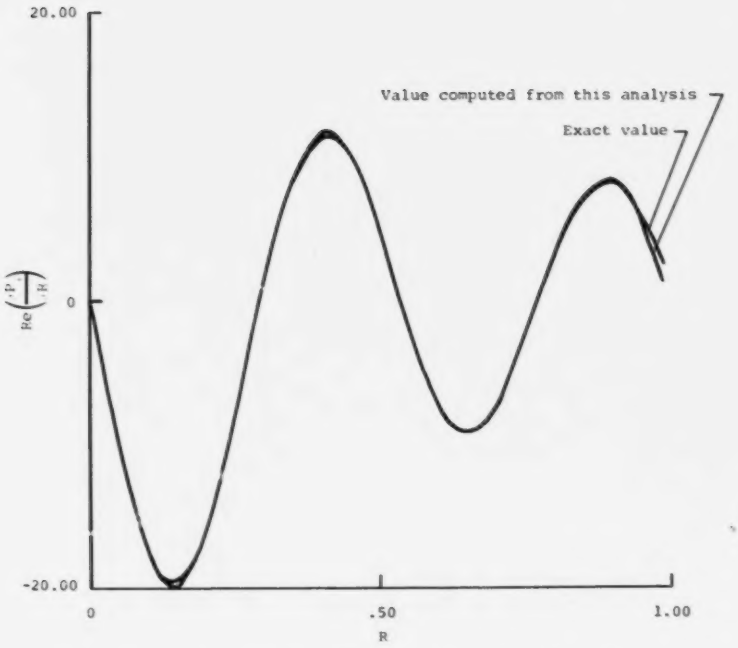

Figure 18.- Real part of radial derivative of the $\ell = 4$ radial mode for $K = 2$, $\beta = 1.54 - 1.29i$, and $\lambda_\ell = 13.122 - 0.23i$.

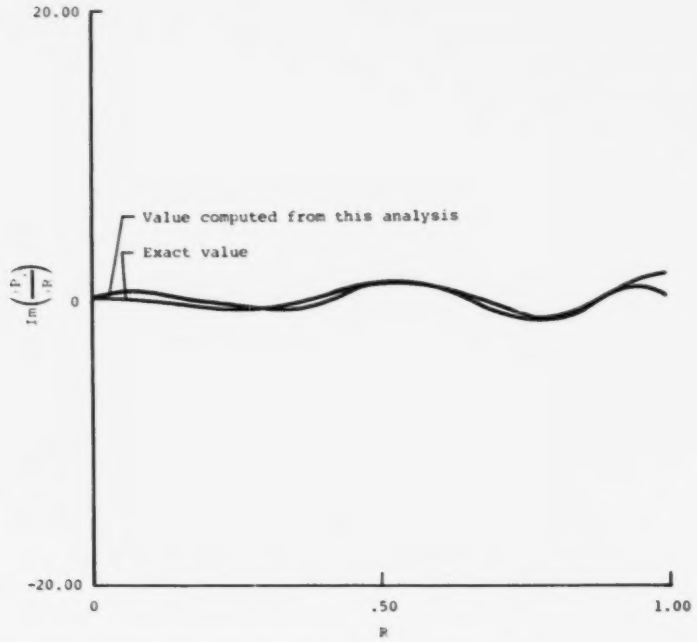

Figure 19.- Imaginary part of radial derivative of the $\ell = 4$ radial mode for $K = 2$, $\beta = 1.54 - 1.29i$, and $\lambda_\ell = 13.122 - 0.23i$.

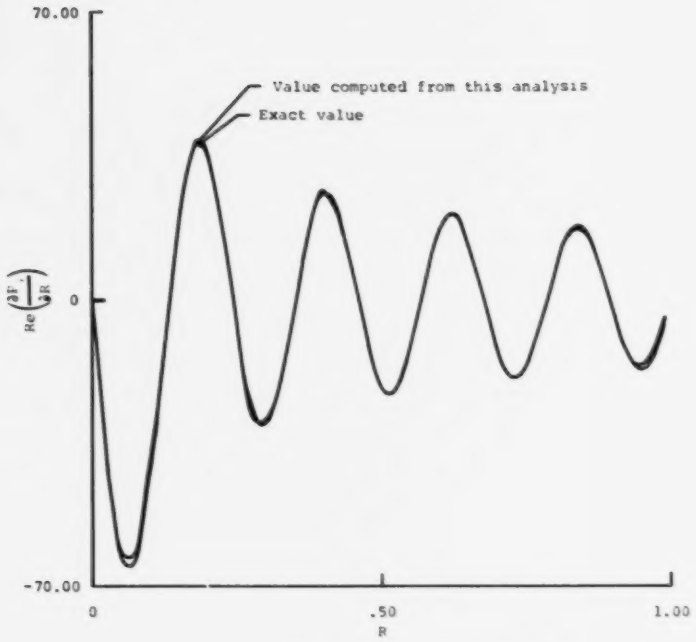

Figure 20.- Real part of radial derivative of $\ell = 9$ radial mode for $K = 2$, $\beta = 1.54 - 1.29i$, and $\lambda_\ell = 28.954 - 0.106i$.

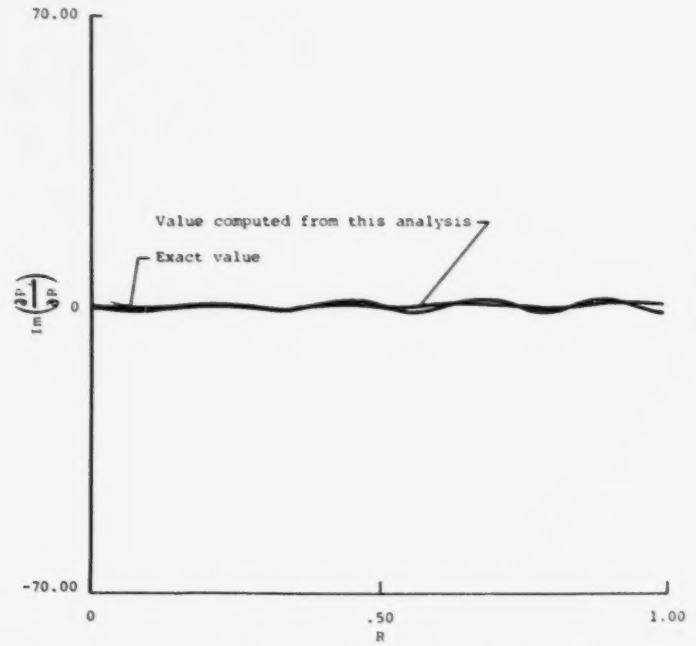

Figure 21.- Imaginary part of radial derivative of $\ell = 9$ radial mode for $K = 2$, $\beta = 1.54 - 1.29i$, and $\lambda_\ell = 28.954 - 0.106i$.

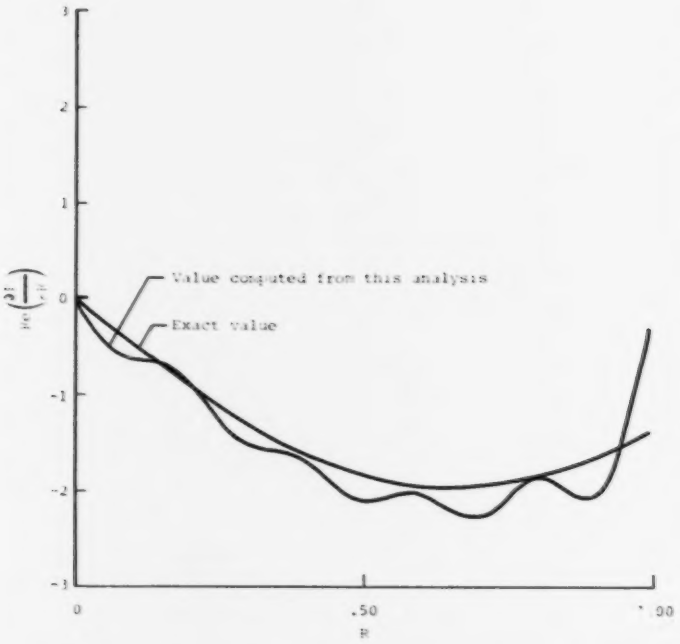

Figure 22.- Real part of radial derivative of $\ell = 0$ radial mode for $K = 10$, $\beta = 0.21 - 0.45i$, and $\lambda_\ell = 2.865 - 0.194i$.

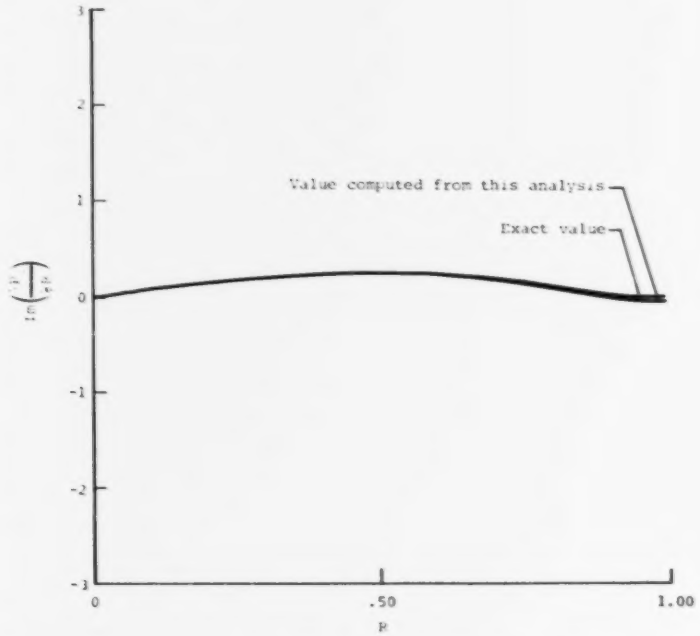

Figure 23.- Imaginary part of radial derivative of $\ell = 0$ radial mode for $K = 10$, $\beta = 0.21 - 0.45i$, and $\lambda_\ell = 2.865 - 0.194i$.

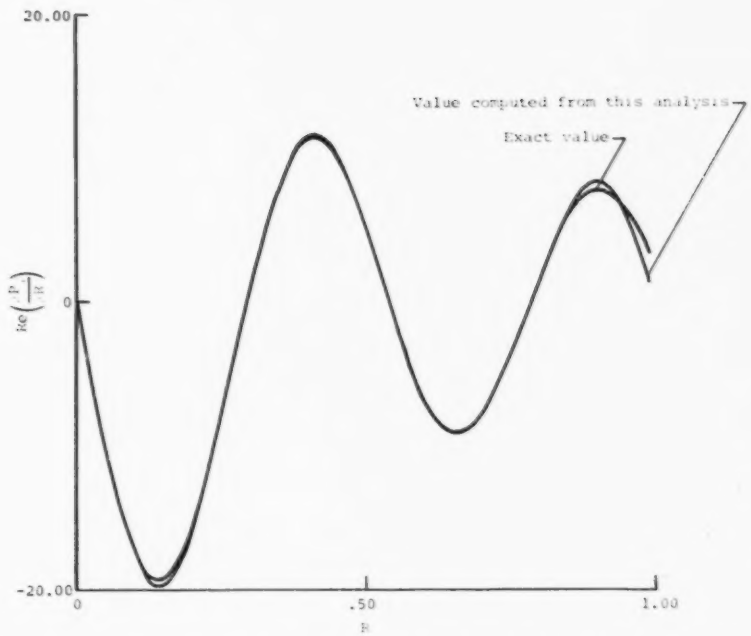

Figure 24.- Real part of radial derivative of $\ell = 4$ radial mode for $K = 10$, $\beta = 0.21 - 0.45i$, and $\lambda_\ell = 12.988 - 0.145i$.

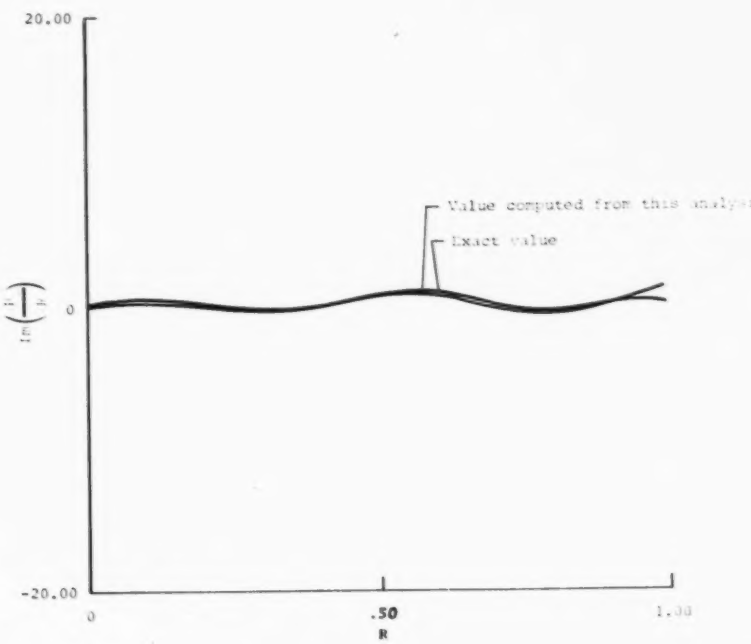

Figure 25.- Imaginary part of radial derivative of $\ell = 4$ radial mode for $K = 10$, $\beta = 0.21 - 0.45i$, and $\lambda_\ell = 12.988 - 0.145i$.

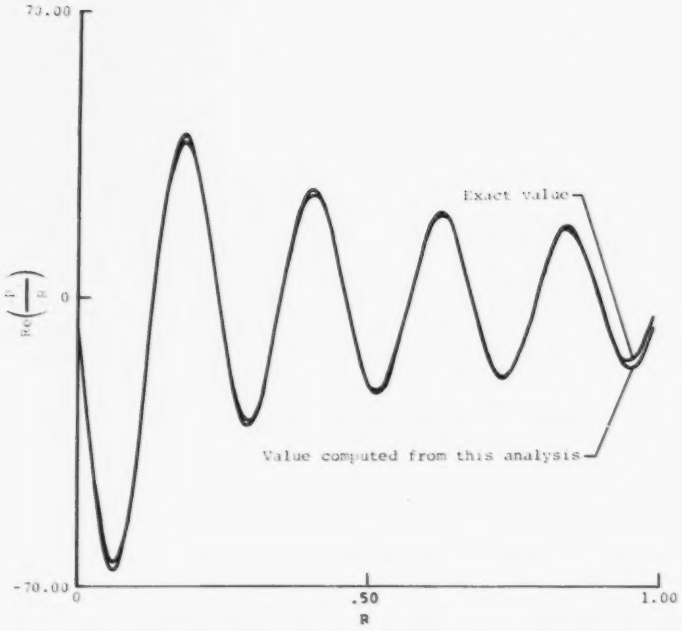

Figure 26.- Real part of radial derivative of $\ell = 9$ radial mode for $K = 10$, $\beta = 0.21 - 0.45i$, and $\lambda_\ell = 28.892 - 0.017li$.

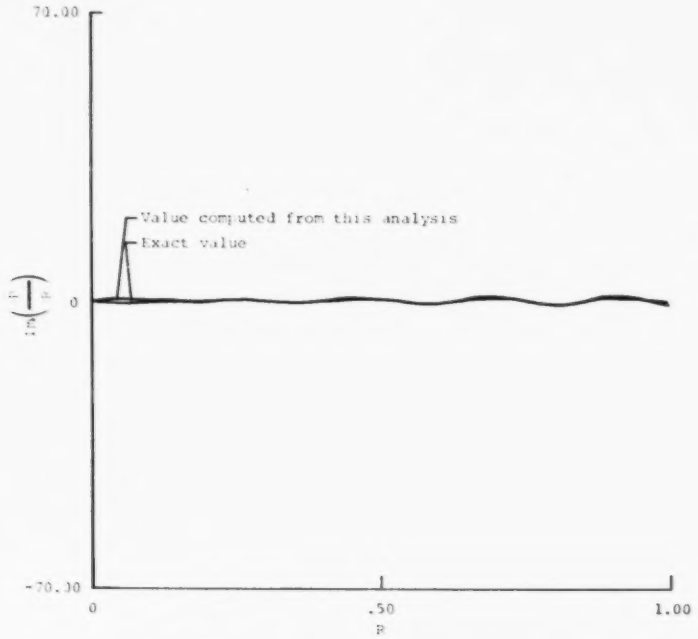

Figure 27.- Imaginary part of radial derivative of $\ell = 9$ radial mode for $K = 10$, $\beta = 0.21 - 0.45i$, and $\lambda_\ell = 28.892 - 0.071i$.

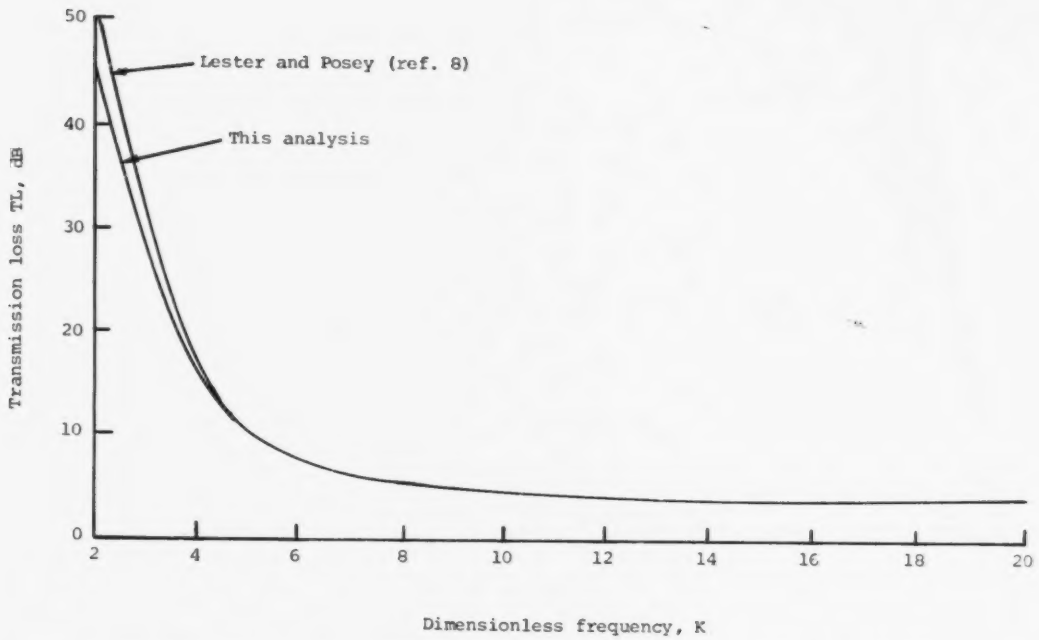

Figure 28.- Comparison of transmission loss predicted at optimum admittance for plane-wave source.

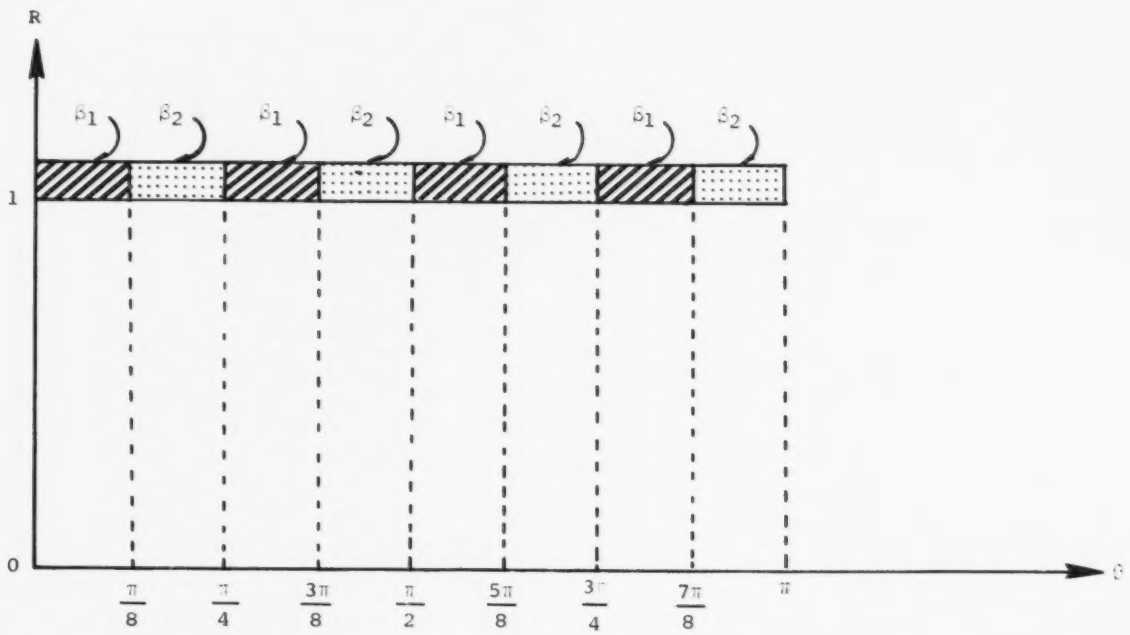

Figure 29.- Even peripherally segmented liner with eight strips (S = 8).

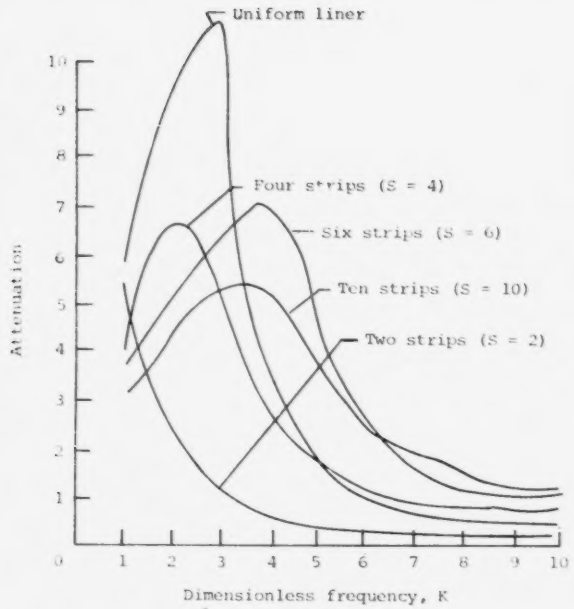

Figure 30.- Least-attenuated mode attenuations for uniform and peripherally segmented liners.

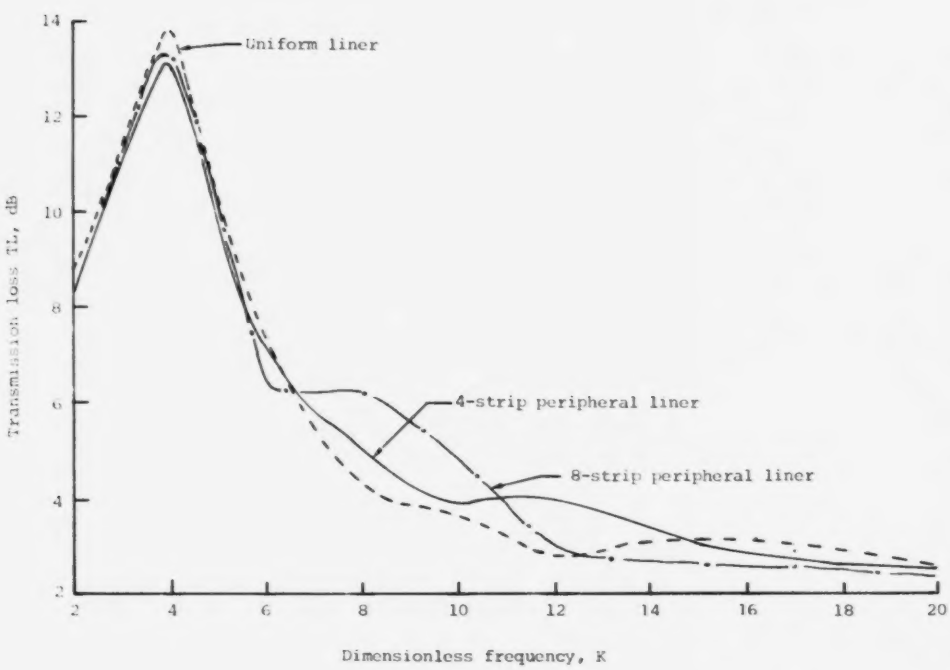

Figure 31.- Comparison of transmission loss of peripheral liner to that of uniform liner tuned at K = 5, for plane-wave source.

1. Report No.	2. Government Accession No.	3. Recipient's Catalog No.
NASA TP-1904		

4. Title and Subtitle	5. Report Date
NOISE SUPPRESSION CHARACTERISTICS OF PERIPHERALLY SEGMENTED DUCT LINERS	September 1981
	6. Performing Organization Code: 505-32-03-06
7. Author(s): Willie R. Watson	8. Performing Organization Report No.: L-14521
	10. Work Unit No.
9. Performing Organization Name and Address: NASA Langley Research Center, Hampton, VA 23665	11. Contract or Grant No.
	13. Type of Report and Period Covered: Technical Paper
12. Sponsoring Agency Name and Address: National Aeronautics and Space Administration, Washington, DC 20546	14. Sponsoring Agency Code

15. Supplementary Notes

16. Abstract

The acoustic fields and transmission losses produced in semi-infinite circular ducts with peripherally segmented liners are analyzed using a series expansion of hard-wall duct modes. The coefficients of the series are computed using Galerkin's method. Unlike finite element approaches, this analysis includes the effects of realistic sources and the number of peripheral strips need not be small. It is shown that peripherally segmented liners redistribute the acoustic energy in waves composed of only a single circumferential mode at the source into other waves which contain a multitude of circumferential modes in the lined section. The accuracy of eigenfunctions computed from the analysis was observed to increase as either the frequency or radial mode order increased. The transmission losses were found to be accurate at frequencies above the cut-on value of the first-order radial mode in a hard-wall duct. The results show that, for plane-wave sources, peripherally segmented liners may attenuate as much sound as an optimized uniform liner at the optimal point while giving more noise suppression at most other frequencies.

17. Key Words (Suggested by Author(s))	18. Distribution Statement
Circumferentially segmented liners Galerkin method Variable boundary conditions Two-dimensional eigenvalue problems	Unclassified - Unlimited Subject Category 71

19. Security Classif. (of this report)	20. Security Classif. (of this page)	21. No. of Pages	22. Price
Unclassified	Unclassified	41	A03

For sale by the National Technical Information Service, Springfield, Virginia 22161

NASA-Langley, 1981